Electron-conducting quantum dot solids: novel materials based on colloidal semiconductor nanocrystals†

Daniël Vanmaekelbergh* and Peter Liljeroth

Received 13th October 2004
First published as an Advance Article on the web 17th February 2005
DOI: 10.1039/b314945p

We review the optical and electrical properties of solids that are composed of semiconductor nanocrystals. Crystals, with dimensions in the nanometre range, of II–VI, IV–VI and III–V compound semiconductors, can be prepared by wet-chemical methods with a remarkable control of their size and shape, and surface chemistry. In the uncharged ground state, such nanocrystals are insulators. Electrons can be added, one by one, to the conduction orbitals, forming artificial atoms strongly confined in the nanocrystal. Semiconductor nanocrystals form the building blocks for larger architectures, which self-assemble due to van der Waals interactions. The electronic structure of the quantum dot solids prepared in such a way is determined by the orbital set of the nanocrystal building blocks and the electronic coupling between them. The opto-electronic properties are dramatically altered by electron injection into the orbitals. We discuss the optical and electrical properties of quantum dot solids in which the electron occupation of the orbitals is controlled by the electrochemical potential.

1. Scope of the review

Crystalline solids can be classified according to their electronic properties. Due to the strong electronic coupling of the atomic orbitals, a solid is characterised by quasi-continuous bands consisting of levels closely spaced in energy. The number of levels in a band is equal to the number of atoms in the crystal.

† This work is dedicated to Professor A. Henglein, a pioneer in chemistry and physics of nanometre-sized crystals.

*daniel@phys.uu.nl

Insulators have bands that are either completely filled or completely empty. The highest filled band is called the valence band; the next higher energy band is called the conduction band; see Fig. 1. For insulators, the forbidden energy gap between those two bands is at least ten times the thermal energy k_BT. This means that electrons cannot be thermally excited from the valence to the conduction band. Furthermore, excitation of the valence electrons in an (arbitrary small) electric field is also not possible, *i.e.* the electrical conductivity is zero. In contrast, metals are characterized by an incompletely filled valence band. This means that electrons can be

Daniël Vanmaekelbergh

Prof. Dr. Daniël Vanmaekelbergh, Chair in Chemistry and Physics of Nanostructures, Debye Institute, University of Utrecht.
I was born in Brugge (Belgium) a long time ago. After finishing the undergraduate chemistry courses at the University of Gent (1980), I was engaged in postgraduate research dealing with photo-electrochemical reactions at semiconductor/electrolyte junctions. Having received my PhD degree and survived my military service I joined the group of Prof. Kelly as an associate professor (1989–2002) and directed my research towards the optical and electrical properties of macro- and nano-porous semiconductors. I am very happy to lead a group of enthusiast young scientists dedicated to the design of quantum dots, artificial quantum-dot molecules and solids, and the study of their opto-electrical properties.

Peter Liljeroth

Dr. Peter Liljeroth, a regular post-doc, Debye Institute, University of Utrecht.
I was born in Lahti, Finland and graduated from the Department of Chemical Technology of Helsinki University of Technology (HUT). I completed my doctorate (2002) under the supervision of Prof. Kyösti Kontturi, concentrating on the electrochemistry at liquid–liquid interfaces. Under the influence of Dr. Bernadette Quinn, I became increasingly interested in ''things'' on smaller scales and joined Prof. Vanmaekelbergh's group as a post-doc within an EU funded RTN-network ''NANOSPECTRA''. At the moment my research interests include, but are not limited to, electronic transport in metal and semiconductor nanoparticle assemblies and scanning tunneling microscopy and spectroscopy on individual nanostructures.

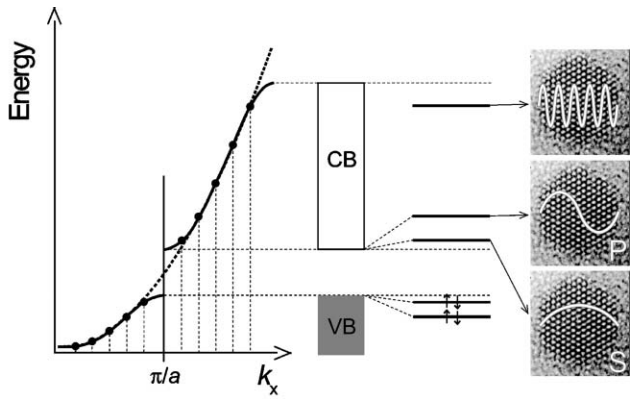

Fig. 1 Relation between the electronic structure of a macroscopic semiconductor and a semiconductor nanocrystal. Left: The dispersion relationship between electronic energy and electron wavenumber k (for the x-direction). Due to scattering of the electrons with the periodic potential of the crystal lattice, electronic bands are separated by forbidden energy gaps. A "band" is a collection of energy levels separated by very small spacings. Middle-left: The completely filled valence band and completely empty conduction band of a macroscopic insulator crystal. Middle-right and right: In a crystal with dimensions in the nanometre range, electrons with low wavenumbers experience quantum confinement: the electron wave has to fit in the limited space of the crystal. Bottom-right: The electron orbital with S symmetry (LUMO), and the second level which has P symmetry. Top-right: The energy levels located at higher energy in the band have many nodal planes; there is only weak confinement. This is typical for the valence electrons in a metallic nanocrystal.

thermally and electrically excited, and, thus, that the electrical conductivity can be considerably above zero. Insulators can be chemically doped with impurity atoms that are not iso-electronic with the atoms of the host lattice. This may lead to spatially localized energy levels located in the forbidden gap. Thermal excitation of an electron from such an energy level into the conduction band leads to a non-zero concentration of conduction electrons; *i.e.* an n-type semiconductor. On the other hand, if a valence electron is thermally excited into a localized band gap level, this results in an empty level in the valence band, which is called a valence band hole. Holes are treated similarly to electrons; however, they have the opposite electronic charge. Crystals with a non-zero number of holes in the valence band are called p-type semiconductors.

In the past twenty years, there has been an increasing interest in crystals with very small dimensions, *i.e.* roughly between 1 and 10 nanometres. These nanocrystals are prepared from molecular precursors in a bottom-up approach. Very often, wet-chemical methods are employed leading to colloidal nanocrystals present in dispersion. It is possible to prepare colloidal nanocrystals consisting of noble metal atoms, transition metals and many semiconductor compounds.[1] World-wide, the scientific research dealing with the chemical, optical, electrical, and magnetic properties of colloidal nanocrystals is growing fast; it is one of the most dynamic fields in nanoscience and nanotechnology. There are two general reasons for this. First, nearly all properties of nanometre-sized crystals depend strongly on their size and shape. In other words, the crystal dimensions determine the optical, electrical and magnetic properties of a given compound. Second, colloidal nanocrystals can be considered as chemical building blocks, which can be used for the preparation of larger and more complex architectures, *e.g.* nanocrystal molecules, two-dimensional arrays and three-dimensional assemblies. In the literature, the latter are often called nanocrystal superlattices, nanocrystal solids or quantum dot solids. In general terms, the properties of these architectures depend on the properties of the individual nanocrystal building blocks, and on the chemical, electronic or magnetic coupling between them. The preparation of new materials in two stages, *i.e.* from molecular precursors to nanocrystals, and from nanocrystals to nanocrystal architectures, offers control and versatility.[1–4]

This tutorial review will focus on the electronic properties of nanocrystal solids assembled from semiconductor nanocrystals of the group II, III, IV, V, VI elements, *e.g.* CdX and PbX (X = S, Se, Te), InP, Si *etc*. The interest of such insulator or semiconductor nanocrystals is evident from Fig. 1. Consider, for instance, a CdSe nanocrystal. The valence electrons form the bonds between Cd and Se. There are no conduction electrons present in such a nanocrystal. However, such electrons can be added, one by one, from an external source or by optical excitation. The first electron that is added to a neutral crystal will occupy the LUMO (Lowest Unoccupied Molecular Orbital). The particle wave function has no nodal plane and fills the entire nanocrystal. In analogy with atomic physics, this electron level is called S. This level can accommodate a second electron, with opposite spin. A third electron will occupy the next higher energy level, which has one nodal plane and P-type symmetry. Such few-electron configurations, confined in semiconductor nanocrystals, are known as artificial atoms.[5] A nanocrystal with one, two, or three conduction electrons can be considered as artificial H, He and Li, respectively. Since the electron particle waves are strongly confined in the limited space of the nanocrystal, the kinetic energy of the electrons is considerably larger than in a macroscopic crystal and increases with decreasing dimensions. In the type of nanocrystals considered in this review, there is such a strong quantum confinement that the energy separation between the S and P electron levels can easily be between 100 and 500 meV. In addition, the energy of the optical HOMO-LUMO gap, and thus the photon energy, also increases with decreasing dimensions. The fact that the optical properties of semiconductor nanocrystals can be tailored by the dimensions has sparked the interest of many scientists, since the middle of the eighties.[6]

We will, however, review another intriguing aspect of semiconductor nanocrystals. Such crystals do not contain conduction electrons (nor valence band holes) in the neutral ground state; thus adding electrons has a dramatic effect on the electrical and optical properties. Addition of a single electron to the S-LUMO (see Fig. 1) leads to quenching of the HOMO-LUMO inter-band light absorption. In addition, absorption in the Infra-Red due to an electronic intra-band transition between the S and P conduction levels is observed.[7,8] In a quantum dot solid, the electrical conductivity rises steeply as soon as electrons are added to the conduction levels. It is obvious that the number of conduction electrons per

nanoparticle, n, is a key parameter that determines the electrical and optical properties of a quantum dot solid.[9]

Electrons can be added to semiconductor nanocrystals in a number of different ways. An electron and hole can be formed by a photo-induced HOMO-LUMO transition. The charge of the conduction electron is then compensated by the charge of the hole. The recombination lifetime of this excitation is usually small (in the ps to μs range). This means that the average number of photogenerated electron-hole pairs per nanocrystal is usually smaller than one. The photoconductivity characteristics of quantum dot solids excited in this way have been reported.[10] If one of the photogenerated charge carriers is preferentially scavenged by a reducing or oxidising species, the nanocrystal is left with electrons (or holes) solely, *i.e.* photochemical generation of charge carriers. As electrons and holes are separated into two different phases, the lifetime of the charge carriers in the nanocrystal can be relatively long.[11] Third, electrons can be injected into semiconductor nanocrystals using strong reducing species.[7,8] The oxidized species form then the positive countercharge, compensating the charge of the electrons in the nanocrystals. Fourth, if an assembly of semiconductor nanocrystals is in electrical contact with a metal electrode, electrons can be injected in the conduction levels of the nanocrystals by control of the electrochemical potential. The electron charge is compensated by positive but inert ions present in an electrolyte solution that permeates the pores of the assembly. This intimate compensation of the electronic charge is called ''electrochemical gating''. Since, in this case electrochemical equilibrium conditions prevail, stable systems with a well-controlled number of electrons per nanoparticle can be formed. This method has proven to be highly successful in the study of electron conducting quantum dot solids, the subject of this review.[12–19]

In sections two and three, we briefly consider the two stages in the preparation of quantum dot solids, *i.e.* the synthesis of colloidal nanocrystals, and their assembly into higher architectures. Extended reviews on synthesis and assembly can be found in the literature.[1–4,6] In section four, we will review experiments, which probe electron transport through an individual nanocrystal. This section serves as an introduction to the main subject of this review: the storage and transport of electrons in an assembly of semiconductor quantum dots, discussed in section five.

2. Chemical synthesis of semiconductor nanocrystals

Synthesis of the nanocrystal building blocks is the first step to formation of nanocrystal assemblies. For this, it is desirable to have soluble nanocrystals that are chemically stable, do not aggregate in solution, are free of defects and well-defined in terms of their size, shape and surface chemistry. Despite the impressive number of different materials that could be synthesised, early synthetic routes in aqueous or other polar solvents employing ionic precursors typically yielded unsatisfactory nanocrystals in terms of their stability, defect chemistry or size-monodispersity. However, all of these desired properties are met by colloidal nanocrystals prepared using wet-chemical methods starting from molecular or atomic precursors in organic solvents. In what follows, we will focus on the modern organometallic route that yields high-quality, defect-free, monodisperse nanocrystals.[20]

Modern organometallic synthesis of defect-free nanocrystals

It is well-established that in order to obtain monodisperse nanocrystals, it is required to separate the nucleation and subsequent growth steps.[1,4] A rapid addition of reagents to the reaction vessel raises the precursor concentration above the nucleation threshold. This supersaturation is relieved by a nucleation burst. The fast decrease of the precursor concentration stops nucleation; in addition, a change in temperature or pH can be used. The remaining precursors are then consumed by the growth of the particles. The dispersion in the nanocrystal sizes is determined by the initial nucleation event. If the monomer concentration is high, but below the nucleation threshold, the small particles grow faster and there is ''focusing'' of the size-distribution. On the other hand, at low monomer concentration, the system exhibits a second, distinctive, growth phase called Ostwald ripening or ''defocusing''. In this process, the high surface energy of the smallest particles promotes their dissolution; the resulting material is redeposited on the larger particles.

The requisite supersaturation and subsequent nucleation can be achieved by rapid injection of organometallic precursors into a vigorously stirred hot coordinating solvent, the so-called hot-injection procedure.[20] The temperature of the mixture is sufficient to decompose the precursors resulting in supersaturation which is relieved by nucleation. For example, monodisperse CdSe can be synthesised by quickly injecting a mixture of elemental selenium and dimethylcadmium dissolved in trioctylphosphine (TOP) into a mixture of hot ($\sim$300 °C) trioctylphosphine oxide (TOPO) and hexadecylamine (HDA). Following the injection, the temperature is allowed to drop to prevent further nucleation and subsequently, it is stabilised to the desired growth temperature. The temperature, concentrations of the precursors and the reaction time control the resulting nanocrystal size while an excess of Se over Cd is required for nanocrystals with high luminescence quantum yield.[21] This reaction must be carried out under inert atmosphere in the absence of water and oxygen. The role of the coordinating solvent (surfactant molecules) is threefold: First, to slow down the growth rate, allowing the nanocrystal cores to anneal for improved crystallinity. Second, aggregation of nanocrystals after the synthesis is prevented by steric stabilisation. Third, the electronic surface states are passivated, which is crucial in obtaining luminescent nanocrystals.

At the moment, the hot-injection procedure can be used as a general synthetic route to many different materials, II–VI (CdX, ZnX where X = S, Se, Te), III–V (InAs, GaAs, InP, GaP), IV–VI (PbS, PbSe, PbTe) and IV (Si, Ge). The best optimised procedures yield polydispersities of 5–10% and luminescence quantum yields up to 80%.

Post-synthesis processing: size-selection and ligand exchange

Despite the recent advances in nanocrystal synthesis, for applications requiring ultimate particle monodispersity, nanocrystal post-processing must be employed. A common procedure to narrow the particle size-distribution is the

so-called size-selective precipitation involving the use of a solvent/non-solvent pair (for example, hexane/methanol). To a mixture of solvent and nanocrystals, the non-solvent is added in small steps: due to the changes in solvent polarity, at some point the largest particles are no longer soluble in the solvent mixture and precipitate. The precipitate is then separated from the supernatant and can subsequently be redissolved. Repeated precipitation/redissolution cycles can be used to narrow the standard deviation in nanocrystal size to smaller than 5%, *i.e.* ± 1 lattice constant.

Exchange of the ligands after the synthesis is a convenient method to control the solubility of the nanocrystals (render them hydrophobic/hydrophilic), to control the interparticle separation in assemblies or to introduce chemically reactive groups onto the nanocrystal surface.[20,22,23] Exposure of the nanocrystals to a solution containing an excess of the incoming ligand followed by precipitation will result in a partial exchange of the molecules on the nanocrystal surface. Repeating this cycle allows for a more complete exchange, even if the new capping molecule binds less strongly to the nanocrystal surface than the original ligand.

The nanocrystal surface can also be coated by an inorganic shell following a standard synthesis and size-selection. The inorganic shell is grown by an organometallic method, in a very similar manner as the core has been prepared. If a wider band gap material is used as the shell, nanocrystals with a high photoluminescence quantum yield and good chemical stability can be obtained (for example CdSe/ZnSe core/shell nanocrystals).[1]

3. Preparation of two-dimensional arrays and solids from nanocrystal building blocks

An interesting problem is, what kind of collective properties arise when semiconductor nanocrystals are assembled into close-packed two- and three-dimensional solids. The assembly of metallic nanocrystal building blocks has been studied extensively; however, the methods presented should be equally applicable to semiconductor nanocrystals. The following paragraphs briefly review the most common approaches to assemble quantum dot solids ranging from simple drop-casting to more sophisticated Langmuir and Langmuir–Blodgett techniques.

Nanocrystal solids obtained by deposition from a nanocrystal suspension

The simplest way of obtaining a quantum dot solid is deposition from a nanocrystal suspension, *i.e.* drop-casting, see Fig. 2. This means applying some drops of monodisperse nanocrystals dissolved in a suitable solvent onto a desired substrate, followed by solvent evaporation. The amount of particles determines whether a monolayer or a three-dimensional assembly is formed. The degree of order in the resulting assembly is mainly determined by the rate of solvent evaporation: fast evaporation leads to amorphous QD solids that lack long-range order. On the other hand, sufficiently slow evaporation leads to very high quality nanocrystal superlattices with domain sizes in the micrometre range.

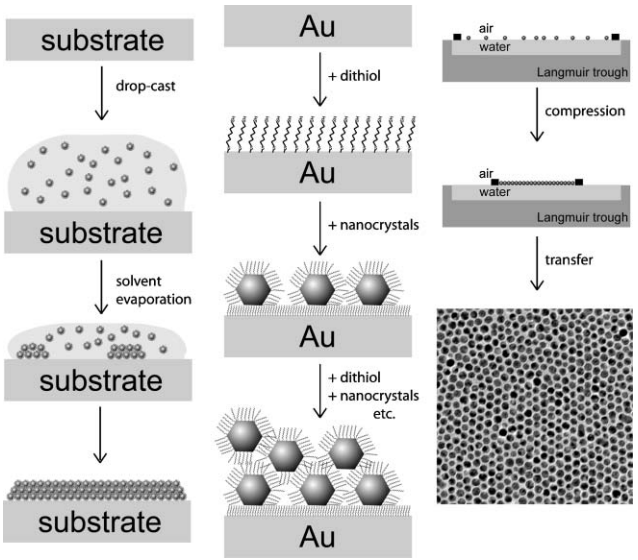

Fig. 2 Different means of preparing quantum dot solids. Left: deposition from a suspension of nanocrystals. Middle: Use of chemical linkers to construct layer-by-layer assemblies of nanocrystals. Right: Preparation of Langmuir–Blodgett monolayers of nanoparticles.

Temperature is another parameter influencing the resulting superlattice quality, higher temperature increases particle mobility which promotes long range order in the assembly.

Controlling the vapour pressure of the solvent over the samples is a much-used method to achieve slow evaporation. Another approach is to add a second solvent of a lower vapour pressure. As the more volatile solvent evaporates, the suspension is very slowly destabilised due to an increase in nanocrystal concentration or a change in solvent polarity. This results in very slow precipitation and both two- and three-dimensional assemblies with long-range order can be achieved.[22] The interparticle spacing in these assemblies is determined by the length of the capping molecules.

If a mixture of particles of two different sizes (A and B) is used, and size and concentration ratios are carefully chosen, it is possible to obtain ordered AB, AB_2, AB_5 or AB_{13} superlattices.[24–26] For example, very high quality binary superlattices (AB_2, AB_5 and AB_{13}) of PbSe and Fe_2O_3 nanocrystals were obtained under controlled atmosphere at an elevated temperature (~ 60 °C).[26]

The properties of the as-prepared quantum dot solids can be altered by post-deposition treatments. For example, exposing the film to a solution of bifunctional molecules can be used to cross-link the nanocrystals in order to improve the mechanical properties of the film and the electronic coupling between the particles.[27] Heating of the film under inert atmosphere or vacuum results in partial or complete desorption of the capping molecules and consequent change in the interparticle separation in the film.

Two-dimensional arrays of nanocrystals with controlled structural properties

An alternative approach in manufacturing ordered monolayers of nanocrystals is the use of the Langmuir–Blodgett (LB)

technique.[2,28] This involves spreading a known amount of a solution of nanocrystals onto an air/water interface in a Langmuir trough (Fig. 2). Once the solvent has evaporated, movable barriers can be used to control the area of the trough and hence the available area per nanocrystal. Simultaneous measurement of the surface pressure gives information on the interactions between the particles. The pressure–area relationship for this two-dimensional system is, in fact, analogous to the P,V-relationship for a three-dimensional system. At large area per particle, the nanocrystals do not interact and the surface pressure is zero. As the film is compressed, the particles are brought into contact and the surface pressure is increased. At a certain compression, the film can no longer support the lateral pressure and collapses into a three-dimensional, disordered, layer. Compression of the film to a given surface pressure (and thus, interparticle separation) can be followed by the transfer of the film onto a solid substrate, leaving the structure intact.

Layer-by-layer formation of three-dimensional solids

Nanoparticle mono- and multilayers can also be constructed using chemical linkers. The idea is to use bifunctional molecules. As a stereotypical example, first an alkane dithiol monolayer is assembled on a gold substrate followed by an exposure to a nanoparticle suspension. Long exposure results in a formation of a saturated monolayer, which still has significantly lower particle density than is found in nanocrystal superlattices. Repeated exposure to bifunctional linkers and nanocrystals makes it possible to build nanocrystal multilayers in a layer-by-layer fashion (see Fig. 2). Dithiol or diamine molecules are typically used as the linker molecules, but it is also possible to utilize carboxylic acid derivatized particles and to use divalent cations as the linkers. In addition, layer-by-layer assembly of nanocrystals with charged ligands can be achieved by using oppositely charged polyelectrolytes as a molecular glue. Finally, for higher packing densities, repeated LB deposition can be used to build up nanocrystal multilayers.

4. Electron addition to a single nanocrystal: artificial atom

In the introduction it was emphasized that nanocrystals composed of the group III–V, II–VI and IV–VI elements are insulators in the uncharged ground state. However, such crystals form a potential well for electrons giving a number of bound conduction energy levels. Thus, electron addition to an otherwise neutral crystal can lead to stable few-electron configurations, which are called artificial atoms. Here, we will consider the energy of artificial atoms strongly confined in semiconductor nanocrystals, which is determined by the single-electron energy levels and electron–electron Coulomb and spin interactions.

Single-electron energy levels

Due to the confinement of the electron particle waves in the limited space of the nanocrystal, the single-electron energy levels (*i.e.* the energy levels of a system that contains only one electron) depend strongly on the size and shape of the nanocrystal. This effect is called quantum-size confinement. Of course, the energy levels are also determined by the chemical nature of the semiconductor crystal, the crystal structure and the energy barriers around the crystal. The single-electron energy levels of a nanocrystal can be calculated on the basis of the time-independent Schrödinger equation, using several degrees of sophistication. The simplest model considers an electron in an empty rectangular box, with infinite energy walls. This example is outlined in Fig. 3. In the case of a spherical box, the wave functions and eigenvalues follow from the Schrödinger equation expressed in polar coordinates. In general, the energy levels are defined by three quantum numbers and the kinetic energy rises with $(\text{size})^{-2}$. This type of empty-box model provides a basic understanding of the symmetry of the lowest conduction orbitals and the relationship between the single-electron electronic structure (density of states) and the symmetry of the box (see Fig. 3). In the methods based on the effective mass approximation, scattering of the electrons with the crystal lattice is taken into account. This model is based on a realistic band structure (see Fig. 1). The calculations of the optical HOMO-LUMO gap, and the conduction electron and valence hole levels are in qualitative agreement with experimental results. Usually, the effect of quantum confinement on the energy of the levels is overestimated. In state-of-the-art calculations, the tight-binding[29] and pseudo-potential[30] methods are used for calculation of the single-electron wave functions and corresponding energies. Both methods are based on realistic band-structures and they take into account the real crystal lattice, including the surface atoms (corresponding to finite energy barriers), and a realistic nanocrystal shape with facets. There is, usually, quantitative agreement between the calculated energy level structure and experimental results. The single-electron wave functions can be used to calculate the electron–electron Coulomb and spin interactions, and the strength of optical transitions. All methods agree on the symmetry and degeneracy of the first conduction energy levels. For crystals with a wurtzite or

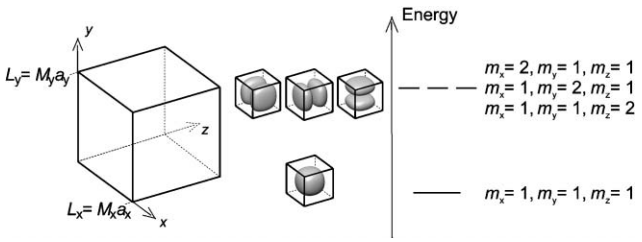

Fig. 3 Orbitals and energy levels for electrons in a empty cubic box. This figure shows the orbitals and energy eigenvalues of an electron confined in a cubic vacuum box surrounded by infinite energy walls. The orbitals and corresponding eigenvalues can be calculated by solution of the time-independent Schrödinger equation. Alternatively, one considers the standing waves in three independent directions x, y, and z. For instance in the x-direction, the crystal has a size $M_x a_x$. (M_x is the number of atoms in the x-direction and a_x the size of the unit cell in this direction). Standing particle waves are possible if $m_x(\lambda/2) = M_x a_x$ with (m_x = 1, 2, …). Thus, wave vectors in the x-direction obey: $k_x = m_x\pi/M_x a_x$. The kinetic energy of the electrons is then given by $E(m_x,m_y,m_z) = [\hbar^2\pi^2/(2m_e)][m_x^2/(M_x a_x)^2 + m_y^2/(M_y a_y)^2 + m_z^2/(M_z a_z)^2]$. The first orbitals and corresponding energy levels are shown.

zincblende crystal lattice and a (nearly) spherical shape with quantum-confinement in three dimensions, the first three levels are, in order of increasing energy: an S level (two-fold degenerate), a P level (six-fold degenerate) and a D level (10-fold degenerate). A four times higher degeneracy holds for crystals with a rock-salt lattice, such as PbS and PbSe nanocrystals.[31,32]

A comparison between the calculated energy levels and the results obtained with optical or electrical measurements is not straightforward. The reason for this is that the electrons or holes have charge and spin. Thus, Coulomb and spin interactions between the electrons in the quantum dot must be taken into account for a correct interpretation of absorption and luminescence spectra, resonant tunneling spectra, *etc*.[33] This will be addressed in the next section.

There is, however, one type of experiment, where electron–electron interactions only play a minor role, namely transitions of electrons (holes) between the conduction (valence) energy levels. Consider, for instance, a three-fold charged nanocrystal with two electrons in the S and one electron in the P-level (thus artificial Li). Electronic transitions from the S or P level to the higher energy levels are possible, in principle. In such a transition, the number of electrons in the nanocrystal remains unchanged. It is thus reasonable to assume that, for intra-band transitions, the Coulomb repulsion energy is (nearly) constant. The total spin of the artificial atom may change, but the exchange energy is only a small contribution to the total electronic energy of the artificial atom. We conclude that from absorption spectra probing electronic intra-band transitions, the single-electron energy-separation between two levels can be obtained. The first results, obtained with CdSe quantum dots were reported by Guyot-Sionnest and collaborators.[7,8] Electron injection into the S-orbital of CdSe nanocrystals present in an organic solution (oxygen- and water-free) was achieved by electron transfer from the strong reducing agent sodium biphenyl. The absorption spectra in the mid-infra red recorded the S to P electronic transition. There was no sign of transitions to higher energy levels, *i.e.* S → D, *etc*. did NOT occur. The energy separations between the S and P level, measured as a function of the diameter of the CdSe quantum dot, were in agreement with the values calculated by the effective mass approximation.

We have studied the intra-band transitions in electron charged ZnO nanocrystals.[11] ZnO nanocrystals in ethanol were charged by a photochemical technique (see introduction). In addition, ZnO nanocrystals present in an assembly were electrochemically charged (see section five). It was possible to occupy the S and P levels of the ZnO quantum dots. By a careful analysis of the spectra, as a function of the occupation number n of the quantum dots, we could detect the S → P, P → D and several other transitions. As in the case of CdSe nanocrystals, only transitions where the angular quantum number l changed by unity were observed. Thus, the optical transitions in artificial atoms follow the same selection rules as in ordinary atoms. The atom-like envelope functions S, P, … provide a true physical description of confined few-electron configurations. In Fig. 4, the energy of the single-particle S, P and D levels of ZnO nanocrystals of variable diameter are presented. They are calculated with a

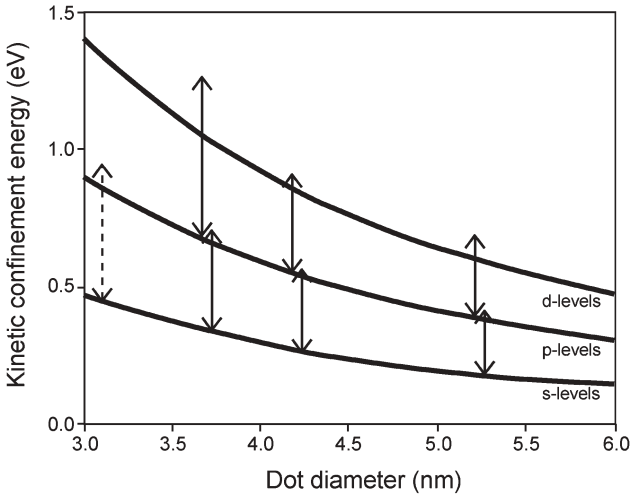

Fig. 4 The energy of the first three single-electron energy-levels (S, P, D in order of increasing energy) of ZnO quantum dots (wurtzite crystal structure) calculated by tight-binding theory as a function of the diameter of the nanocrystals. The arrows indicate the energy separations between the S and P and P and D levels obtained from mid-infra red absorption spectra from electron-charged nanocrystals. Full arrows: uncapped ZnO nanocrystals,[11] dashed arrow: Alkane capped ZnO quantum dots.[29]

sophisticated tight binding method, which also accounts for the facets of the wurtzite nanocrystals and the surface termination of the Zn atoms (Zn–OH). The separations between the S and P and P and D levels, as obtained from absorption spectra, are denoted by arrows. We include the result obtained with capped ZnO nanocrystals by Guyot-Sionnest and co-workers.[34] It can be seen that the measured energy separations increase with decreasing size of the quantum dots; the separations are slightly but systematically larger than the calculated values. In a recent paper, also intra-band absorption in PbSe quantum dots has been studied.[35] At the end of this section, it should be remarked that emission of photons due to intra-band relaxation has not yet been observed.

Building up artificial atoms

Electrons have charge and spin. This means that the total energy of artificial atoms will be determined by the single-electron energy levels, and the Coulomb and spin interactions between the electrons (or holes). Zunger and co-workers have discussed this in great detail.[33] They presented a theoretical framework that allows the comparison of (quantum-mechanical) calculations directly with experimental electron-charging. We will present here a simplified version of the theory by neglecting spin-interactions and assuming that the electron–electron repulsion interactions are independent of the angular quantum number. This framework is sufficient to understand most of the experimental results on charging individual quantum dots and their assemblies (as discussed in the following section).

The sequential addition of electrons in a semiconductor nanocrystal is shown in Fig. 5. If we add the first electron into an otherwise neutral semiconductor nanocrystal in the ground

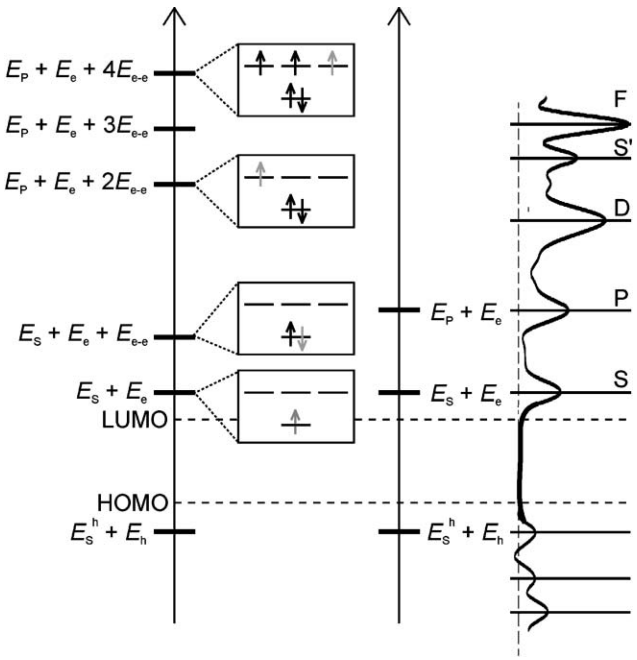

Fig. 5 Building up artificial atoms that are strongly confined in a semiconductor nanocrystal. We consider a nanocrystal, with S (LUMO) and P single-electron levels, and a HOMO hole level, the HOMO-LUMO band gap is not drawn on scale. On the left axis, the electrochemical potentials are given for sequential addition of one electron (indicated in gray) to these energy levels. The first and second electron is added to the S level, the third to eighth electron to the P levels. These electrochemical potentials are relevant in the case of shell-filling spectroscopy. The electrochemical potential for addition of the first hole is also indicated. On the second axis, the energies for adding a single electron to the S and P levels of an unoccupied crystal are indicated. These energies are relevant in shell-tunneling spectroscopy and are close to the single-electron energy levels. On the right, an experimental shell-tunneling spectrum of a CdSe nanocrystal is shown, indicating, the energies for tunneling through the S, P, D, … levels.

state, to a single-electron energy level E_S (this is the LUMO), the electron charge will polarize the dielectric medium of the nanocrystal (dielectric constant ε_{in}) and the dielectric environment (ε_{out}). Due to the fact that the dielectric screening length is larger than the radius of the nanocrystal, the charge of the incoming electron induces a negative charge density on the nanocrystal surface. The repulsion between the electron charge and induced surface charge is accounted for by the self-energy or charging energy E_e. Thus, the electron addition energy for adding the first electron is:

$$\tilde{\mu}(0/1) = E_S + E_e \quad (1)$$

(In this equation and the subsequent ones, energies E have positive values.) In the case that electrons are added to a single nanocrystal, the electron addition energy has the same meaning as the electrochemical potential. The above equation thus gives the potential (of a source electrode) at which electron injection into a nanocrystal begins. If we wish to add a second electron to the nanocrystal, we have to take into account that there is not only dielectric charging, but also a Coulomb repulsion between the incoming electron and the electron already present in the LUMO. The latter energy is denoted as E_{e-e}. The electrochemical potential necessary to add the second electron in the nanocrystal is thus:

$$\tilde{\mu}(1/2) = E_S + E_e + E_{e-e} \quad (2)$$

A third electron will occupy the P energy levels. This incoming electron will interact with the two electrons already present in the S-level. The electrochemical potential is thus:

$$\tilde{\mu}(2/3) = E_P + E_e + 2E_{e-e} \quad (3)$$

In a spherical nanocrystal, there are three P levels that can accommodate 6 electrons in total. The electrochemical potentials can be written in a similar way as presented above. The ladder of electron addition energies (hole addition energies) is presented schematically in Fig. 5. The total energy of an artificial atom or electron-hole exciton can be obtained directly by summing up the electron (hole) addition energies. For example, the ground state exciton is composed of an electron in the LUMO and a hole in the HOMO that experience Coulomb attraction. Neglecting again the spin of the particles, the exciton energy can be found by first adding an electron to the LUMO (addition energy $E_S + E_e$) and then adding a hole to the negatively charged nanocrystal (addition energy $-E_S^h + E_h - E_{e-h}$). The optical gap of a nanocrystal is thus given by:

$$\hbar\omega = (E_S - E_S^h) + (E_e + E_h - E_{e-h}) \quad (4)$$

$(E_S - E_S^h)$ is the single-particle band gap of the nanocrystal, determined by quantum confinement. $(E_h + E_e - E_{e-h})$ is the electron-hole attraction energy (negative), also called exciton-binding energy, and is determined by the electron and hole wave functions and the dielectric constant of the nanocrystal. Since $(E_h + E_e)$ is nearly compensated by E_{e-h}, the electron-hole attraction energy forms only a small correction to the single-particle band gap.

Scanning tunneling spectroscopy of individual nanocrystals

Electron addition to an individual nanocrystal can be studied by capacitance measurements. In practice, with nanocrystals, scanning tunneling spectroscopy is used. The nanocrystals are bound to a conducting substrate by a monolayer of end-functionalized organic molecules. The tip of the STM is placed above the crystal. A bias V is applied between the tip and the substrate. The current between the tip and substrate is due to resonant tunneling from the tip to an energy level of the nanocrystal, and subsequent tunneling from the crystal to the substrate electrode (or *vice versa*). Thus the steps in the current–potential plot reflect the resonant energy levels of the nanocrystal (Tunneling Spectroscopy).

Scanning tunneling spectroscopy was first performed with metallic nanocrystals. In the case of a metallic nanocrystal, the single-electron levels are separated by a very small energy ($\ll k_BT$). Thus, the electrochemical potentials for sequential electron charging are separated by the Coulomb-repulsion energy E_{e-e} [see eqn. (1)–(3)]. Single-electron charging and

tunneling can occur if $E_{e-e} > k_BT$. This is known as "Coulomb-Blockade" single-electron tunneling.[36]

Tunneling spectroscopy on semiconductor nanocrystals started only quite recently. Banin and co-workers reported the first encouraging results (obtained at cryogenic temperatures) on electron addition to an individual InAs colloidal nanocrystal, attached to a gold substrate by hexane-dithiol molecules.[37] The tunneling spectrum (*i.e.* $\partial I/\partial V$ plotted as a function of the bias V) showed the sequential injection of two electrons into the S, and 6 electrons into the P levels of the nanocrystal. Artificial atoms consisting of one, two, …, eight electrons could thus be studied. Such efficient electron charging is due the fact that in this case tunneling from the tip into the InAs nanocrystal was (much) faster than tunneling from the nanocrystal to the substrate. The occupancy of the nanocrystal is determined by the electrochemical potential of the tip (source) electrode. This type of spectroscopy is conveniently called shell-filling spectroscopy, and is similar to capacitance spectroscopy. On the other hand, we have shown that if the conditions of tunneling are changed; *i.e.* if tunneling into the nanocrystal is much slower than tunneling out, the nanocrystal is either empty or charged with one electron.[38] If the bias is increased, electrons tunnel resonantly to the S, P, … levels, without electron–electron interactions taking place. The energies of resonant tunneling are thus determined by the single-electron energy levels $E_S + E_e$, $E_P + E_e$, *etc*., *i.e*. shell-tunneling spectroscopy (see Fig. 5, right potential axis). Such a shell-tunneling spectrum ($\partial I/\partial V$ *vs*. V) is shown in Fig. 5, obtained with a single CdSe nanocrystal (4.3 nm in diameter). The resonance peaks indicate tunneling through the S, P, … levels, hence, the separations between the energy levels can be obtained. At opposite bias, the peaks indicate tunneling of holes through the discrete valence levels of the CdSe dot.

Scanning tunneling spectroscopy with an STM offers great versatility to study the single-electron energy levels and electronic interactions in a single colloidal nanocrystal, and to study few-electron artificial atoms. In the next section, the electronic properties of nanocrystal assemblies will be considered in more detail.

5. Electron addition to a nanocrystal solid

Electronic interactions in a nanocrystal solid

We have seen that due to quantum confinement, semiconductor nanocrystals have a set of discrete conduction electron and valence hole levels. The band gap between the conduction and valence levels and the separations between the individual conduction levels depend on the size and shape of the nanocrystals. These features contribute to the enormous interest in the optical and electrical properties of individual, non-interacting nanocrystals. In addition, such nanocrystals can be considered as building blocks for larger architectures, *i.e.* nanocrystal molecules, 2-D arrays and 3-D quantum dot solids. In these systems, electronic interactions between the nanocrystals must be taken into account. In analogy with the concept of artificial atoms, one may describe these systems as artificial solids. We will also use the term "quantum dot solid" to indicate 3-D assemblies of semiconductor nanocrystals.

A TEM image of a small part of such a solid (here consisting of PbSe nanocrystals) is shown in Fig. 6. It is clear, that unlike in an ordinary solid, the ordering of the atoms in the lattice is not perfect. This has several origins. First of all, there is a distribution in the size and shape of the nanocrystals. Nanocrystals are not truly spherical, it can be seen that they are faceted. Secondly, van der Waals forces between the individual nanocrystals, and between the capping molecules keep the "atoms" in the assembly together. The strength and directionality of van der Waals forces differ strongly from those of covalent or ionic bonds in ordinary solids. The distance between the nanocrystals is mainly determined by the length of the capping molecules, and can be modified by external pressure. We can conclude that quantum dot solids display considerable lattice disorder, accompanied with a variation in the distance between the nanocrystals.

The opto-electronic properties of quantum dot solids will depend on the electronic structure of the individual nanocrystal building blocks, and on their electronic interactions. We will first consider here the important physical phenomena and related energy scales; they will be compared with the thermal energy k_BT at room temperature. Due to quantum confinement, nanocrystals are characterized by discrete energy levels; *i.e.* S, P, D levels. For the crystals discussed in this review, with dimensions in the nanometre range, the confinement is so strong that the energy level separations, *e.g.* $E_P - E_S$, are much larger than k_BT at room temperature. As a consequence, the occupancy of the levels with electrons is not strongly thermally broadened, and artificial atoms are in the electronic ground state. For instance, in a nanocrystal with two electrons, the probability for the ground state, S^2, is much larger than for any excited state. Due to the strong confinement, a distribution in the dimensions leads to a variation in the energy levels of the nanocrystals in the solid, *i.e.* a dispersion in site energy. Consider for instance, ZnO nanocrystals with an average diameter of 4.5 nm. We assume a realistic value of the size dispersion of 10%. From Fig. 4, it follows that the S level of the crystals with a diameter of 4 and 5 nm is 70 meV higher and 50 meV lower, respectively, than the S level of a nanocrystal with a diameter of 4.5 nm. There is thus a variation in the site energies in the order of few k_BT at room temperature. The quantum mechanical coupling between the energy levels can be expressed in terms of a coupling energy (also called level broadening) $h\Gamma$, where h is Planck's constant and Γ the tunneling rate between two orbitals of nanocrystal neighbours. The electronic coupling energy depends strongly on the extension of the orbitals in the nanocrystals, and the width and height of the energy barrier between two nanocrystal neighbours. This means that the nature of the nanocrystals, the capping molecules and possible chemical linkers between the nanocrystals will strongly influence the electronic coupling in a nanocrystal solid. Comparing the electronic coupling energy with the thermal energy two transport regimes can be distinguished (Fig. 6). In the weak coupling regime, $h\Gamma \ll k_BT$; this means that electrons can tunnel between neighbouring dots only. Electron transport occurs by sequential tunneling from dot to dot. The rate of electron transport is influenced by the site disorder, and by Coulomb-effects (self-energy E_e and electron-repulsion E_{e-e}). In the strong coupling regime,

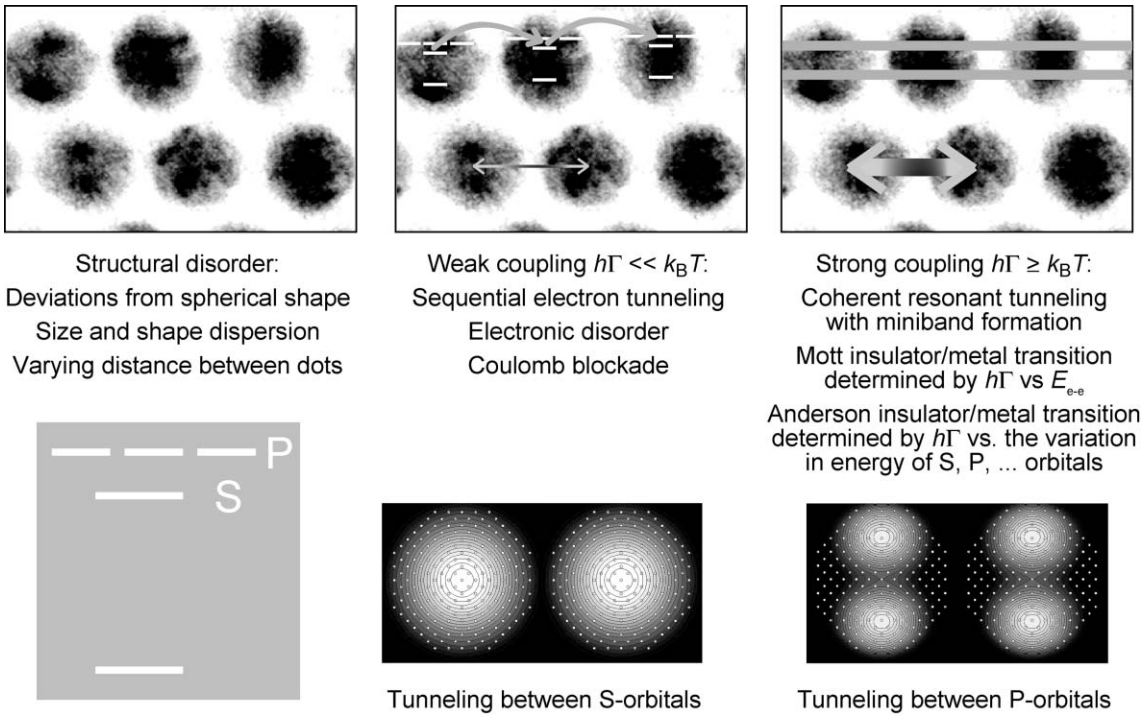

Fig. 6 Electronic interaction in a quantum dot solid. Above-left: A semi-ordered array of nanocrystals displaying structural disorder effects. Centre and right: Sequential electron tunneling in the weak coupling regime and miniband formation in the strong coupling regime. Bottom: The conduction S and P orbitals of a nanocrystal building block that are involved in electronic interactions.

$h\Gamma \geqslant k_BT$; this means that coherent molecular-type orbitals extend over many nanocrystal sites in the solid. Energetically, the discrete orbitals of the nanocrystals form a band of width $h\Gamma$ in analogy to an ordinary crystal. It is important to realize that, for a given quantum dot solid, the regime of strong coupling can, in principle, be reached by a sufficient reduction of the temperature. Remacle and Levine have presented a detailed theoretical framework for the transport characteristics of quantum dot solids in the strong coupling regime.[2,39] A discussion of their results is beyond the scope of this review. We consider here two sub-regimes in the strong-coupling regime. Comparison of the coupling energy $h\Gamma$ with the dispersion in site energies, *e.g.* ΔE_S, defines the Anderson metal–insulator transition: if $h\Gamma$ is larger than ΔE_S, the coupling is sufficiently strong to overcome the dispersion in the energy levels of the individual quantum dots, and extended wave functions still exist. In the opposite case, the system breaks up into small isolated regions where strong coupling prevails, separated by weakly conducting regions. Comparison of the coupling energy $h\Gamma$ *vs.* the Coulomb terms (self-energy E_e and electron-repulsion E_{e-e}) defines the Mott insulator–metal transition. If $h\Gamma$ is larger than E_{e-e}, the coupling energy overcomes electron-localization by Coulomb blockade, and coherent wave functions extend over large regions of the solid. Experiments with two-dimensional arrays of metallic silver and gold nanocrystals have been performed in a broad temperature range. In these systems, the coupling energy can be varied by the interparticle separation. Strong evidence for Anderson and Mott transitions has been presented.[2,40–42]

In three-dimensional quantum dot solids that consist of semiconductor nanocrystals, experimental results point to the regime of weak coupling, except at cryogenic temperatures.[41] These results will be discussed in the next sections. Semiconductor quantum dot solids feature a variety of transport phenomena due to the fact that the occupation of the energy levels can be varied in a controlled way.

Electron injection in a quantum dot solid

In a previous section, we discussed the energy for sequential addition of electrons into a single semiconductor nanocrystal. Here, we consider the injection of electrons in an assembly of nanocrystals. We will treat the case of weak coupling: the density of states is thus composed of the (nearly) unperturbed energy levels of the individual nanocrystal building blocks. We assume, however, that there is sufficient electronic coupling between the nanocrystals in the assembly, such that electrons can diffuse freely by sequential tunnelling (see Fig. 6). These are the conditions that are met in current nanocrystal assemblies. In comparison with electron addition to a single nanocrystal, two additional contributions have to be taken into account. First, the electrons are dispersed over the nanocrystals in the assembly. This "electron dilution" must be accounted for by an entropic contribution to the electrochemical potential for adding the Nth electron, of the form $k_BT \ln(N/N_{tot})$, where N_{tot} is the total number of conduction states in the assembly. Second, electron–electron repulsions will not only occur within a nanocrystal, but also between the electrons present in different nanocrystals. Thus, instead of the Coulomb-contribution $(n-1)E_{e-e}$ in the electron addition energy to a single nanocrystal [see eqn. (1)–(3)], the Coulomb-repulsions of the incoming electron with all electrons

present in the assembly must be accounted for. The electrochemical potential for adding the Nth electron into an S-conduction level in a quantum dot assembly can thus formally be denoted as:

$$\tilde{\mu}(N-1/N) = (E_S + E_e) + \sum_{i=1}^{N-1} E_{e-e}(\vec{r}_N - \vec{r}_i) + k_B T \ln \frac{N}{N_{tot}} \quad (5)$$

Due to Coulomb repulsions, only a very limited number of electrons can be inserted into a nanocrystal assembly, if the charge of the electrons is not compensated by positive charge.

Charge compensation can be achieved in a number of different ways (see introductory section). In a field-effect device, a gate electrode is coupled capacitively to the solid of interest (see Fig. 7). Upon application of a suitable potential difference between the gate and the assembly, V_{gate}, positive surface charges on the gate side of the capacitor occur, compensating the electronic charges in the solid (forming a two-dimensional sheet). The charge density equals CV_{gate}. In the case of nanocrystal assemblies, another type of charge compensation has proven to be successful. Positive, inert ions can be inserted into the voids of the solid. This leads to an intimate and three-dimensional compensation of the electronic charge, see Fig. 7. Such conditions can be realized if the assembly forms the working electrode in an electrochemical

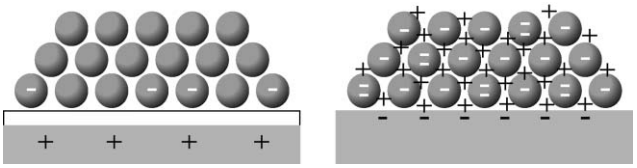

Fig. 7 Different ways of compensation of the electron charge in a quantum dot solid. Left: A gate electrode (gray) is capacitively coupled to the quantum dot solid. Under application of a potential difference, the charge of the electrons in the quantum dots is compensated by the surface charge on the gate electrode. Only the quantum dots closest to the gate can be charged. Right: Electrochemical gating: the charge of the electrons is compensated by inert positive ions present in a liquid that permeates the quantum dot assembly. Here, the situation with one electron per nanocrystal on average is shown.

cell (see Fig. 8). The electrochemical potential of the assembly (which is controlled with respect to a reference electrode by a potentiostat) determines the electron density in the quantum dot solid. Thus, the electron number n (number of electrons per nanocrystal) can be varied between almost zero and a certain maximum number. This maximum number is determined by the potential window in which the assembly is chemically stable (see further). The positive ions inserted in the nanocrystal assembly strongly reduce the electrostatic repulsion between the electrons (contribution $\sum_{i=1}^{N} E_{e-e}(\vec{r}_N - \vec{r}_i)$ to the electrochemical potential), so that the number of electrons that

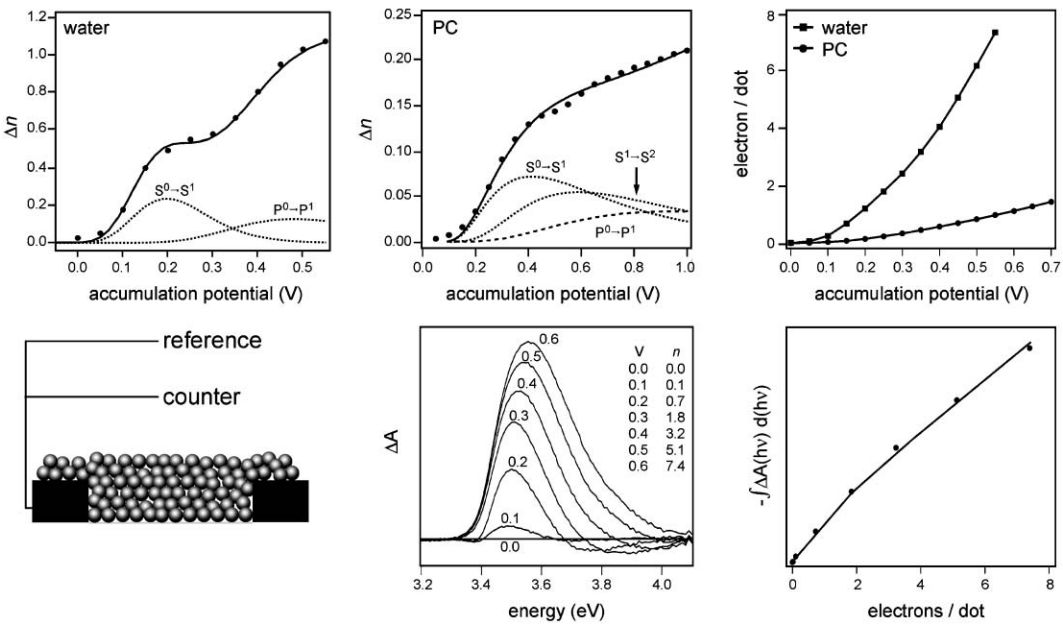

Fig. 8 Electrochemical electron injection in a quantum dot solid. The assembly consists of ZnO nanocrystals of 3.9 nm in diameter, and forms the working electrode of a three-electrode electrochemical cell (below-left). The electrochemical potential determines the electron density in the assembly. Above: The charging characteristics of the ZnO nanocrystal assembly permeated with water and propylene carbonate (PC) electrolyte solutions. Left and middle: Differential capacitance (expressed as the number of injected electrons per crystal for incremental increase in the accumulation potential) *vs.* the accumulation potential in water and PC. Right: Total number of electrons per nanocrystal as a function of the accumulation potential showing the remarkable difference between water and organic solvents (here PC). Below-middle: Quenching of the intraband light absorption in the near UV with increasing electron number. At low electron number the HOMO-LUMO transition (at around 3.5 eV) is quenched, proving that the injected electrons occupy the conduction S orbitals. If $<n>$ rises above two, a second transition is quenched (at around 3.8–3.9 eV), this forms a strong indication that conduction P orbitals are occupied. Below-right: Integrated quenching as a function of the number of electrons per ZnO nanocrystal.

can be injected in the available electrochemical window is strongly enhanced.

Which energy levels are occupied?

Electrochemical charge injection into CdSe, PbSe and ZnO quantum dot solids has been studied experimentally.[9,12–19] A combination of electron charging experiments with *in-situ* inter-band and intra-band light absorption measurements has proven to be very powerful in determining which energy levels are occupied. Such optical measurements can distinguish between the occupation of possible surface states and conduction S and P orbitals. Guyot-Sionnest and co-workers reported quenching of the HOMO-LUMO absorption in CdSe, and a second excitonic transition, proving that the S and P orbitals can become occupied under conditions of electrochemical electron injection. In accordance, IR absorption measurements showed the S → P and P → D transitions upon increasing electron occupation.[18]

We have studied electrochemical electron injection into an assembly consisting of uncapped ZnO nanocrystals of diameter between 3.3 and 5.0 nm. Assemblies permeated with an aqueous and several non-aqueous electrolyte solutions (acetonitrile, propylene carbonate, ethanol) have been investigated.[9,12–14] The (average) electron number n was obtained from measurement of the number of injected electrons and the number of nanocrystals in a given assembly. A comprehensive panel of results obtained with nanocrystals with an average diameter of 3.9 nm is shown in Fig. 8. The differential capacitance (expressed as the number of electrons injected in the assembly per 50 mV increase in the accumulation potential) is shown in the first two plots. With an aqueous solvent, two waves are observed in the potential window. The electron number n increased from zero to eight (upper-right plot). In contrast, when the assembly is permeated with a propylene carbonate solution only one wave is observed, and n is five times smaller. Similar results were obtained with ZnO nanocrystals of 4.3 nm in diameter. The double-wave structure obtained with an aqueous solution can be explained by considering occupation of the S orbitals, followed by occupation of the P orbitals at higher accumulation potential (see Fig. 8). This means that electron injection is determined by the single-electron energies E_S and E_P, and, hence, electron–electron-repulsion is not important [see eqn. (5)]. In contrast, the results obtained with non-aqueous solutions show that occupation of the P orbitals overlaps to some extent with that of the S orbitals. The fact that the electron number is much smaller for the same accumulation potential shows that Coulomb-repulsions play an important role [see contribution $\sum_{i=1}^{N} E_{e-e}(\vec{r}_N - \vec{r}_i)$ in eqn.)5)], despite the insertion of positive counter charges in the voids of the assembly (Fig. 7). In aqueous solvents, charge compensation is apparently much more effective, which will be discussed below. Using optical absorption spectroscopy, we investigated which energy levels become occupied when electrons are injected. The lower panel shows the quenching of the light-absorption in the UV with increasing accumulation potential (decreasing electrochemical potential) for a ZnO assembly permeated with an aqueous solution. The quenching turns on at the same potential where electrons are injected. Between 0.1 and 0.3 V, the HOMO-LUMO (S) transition (at around 3.5 eV) is quenched. At more negative potentials a second quenching signal turns on (at around 3.8 eV). This shows that the S orbitals become occupied if n is between 0 and 2, followed by the occupation of the P orbitals at electron numbers larger than two. The (integrated) quenching signal is zero only when n goes to zero; the same holds for the IR absorption due to the S → P transition. These results give a strong indication that storage of electrons in surface states is not important. This is in accordance with tight-binding calculations of the electronic structure of ZnO nanocrystals, which show that surface states are not located in the band gap of the material.[12]

Why is the Coulomb-repulsion energy smaller than $k_B T$ if the ZnO nanocrystal assemblies are permeated with water? Theory predicts that, in ZnO, interstitial protons form a donor site compensated by a conduction electron.[43] Recently, experimental evidence was reported supporting this theory.[44] In our experiments, protons from the aqueous solvent can be inserted into the lattice, when electrons are injected. Since the protons overlap with the electron wave function, the screening of the electron–electron repulsion is very efficient, and consequently, the Coulomb repulsion energy can become smaller than $k_B T$ at room temperature. This could explain that considerably larger electron numbers can be reached for ZnO nanocrystal assemblies permeated with an aqueous electrolyte solution.

Electron transport in a quantum dot solid

The characteristics of electronic transport in two- and three-dimensional arrays of metallic and semiconductor quantum dots has attracted the interest of many research groups. One of the reasons is that such systems form the analogue of ordinary solids, with artificial atoms replacing the true atoms. In addition, such artificial systems offer a great versatility in a number of important parameters such as the nature of the nanocrystal building blocks and the electronic coupling between them, the screened Coulomb-repulsion, and the disorder parameters. Theorists have explored this parameter space and predicted a number of different transport regimes (see above and Fig. 6). Transport in arrays of metallic quantum dots (Ag or Au nanocrystals) has been investigated in detail and several of the theoretically predicted transport regimes are now supported by sound experimental data.[2,40,42,45] Research with solids composed of semiconductor nanocrystals has only started recently, but the results that have been reported are very encouraging.

Assemblies of semiconductor nanocrystals offer the opportunity to increase the electron number (per quantum dot) gradually from zero. The uncharged ground state is insulating, and one can study the effects of increasing electron number on the characteristics of electron transport. The electron number forms thus another transport parameter, in addition to those cited above. Since the S and P single-electron energy levels are separated by a gap spanning several times the thermal energy at room temperature, insulator/metal transitions can be expected due to shell-filling. In practice, an electrochemical cell is used, similar to the one presented in Fig. 8. The working electrode, however, consists of the quantum dot assembly, bridging a gap between two gold electrodes (source and drain).

The electrochemical potential of this system is controlled with a potentiostat. In addition, a small bias is applied between the two gold electrodes, in order to measure the conductance of the assembly in the linear response regime (current between source and drain proportional to bias). Exciting results have been obtained with assemblies of CdSe nanocrystals of diameters between 5 and 7 nm.[18] The electron number was varied using the electrochemical gating method. From optical measurements, it was shown that the S and P orbitals are filled consecutively. The conductance displayed two peaks with increasing electron number, separated by an almost insulating state. The results were attributed to a sharp transition between two transport regimes, involving S and P orbitals, respectively (see Fig. 9). In the case of weak electronic coupling, electron transport proceeds by tunneling processes between orbitals of neighbouring quantum dots (see Fig. 6). It follows that, for electron numbers smaller than two, transport involves tunneling between S orbitals. One may expect that the electron mobility is proportional to the probability of finding an empty S-orbital in a quantum dot site neighbouring the filled site, $[2 - f(S)]$, where $f(S)$ is the occupation number of the S orbitals. It follows that the conductivity is proportional to $f(S) \times [2 - f(S)]$, thus displaying a peak at around $f(S) = 1$ (see Fig. 9). The mobility and conductivity decrease to zero if all the S orbitals become occupied. A second peak in the conductivity can then be expected when the P orbitals become half-filled. Recent Monte Carlo random-walk simulations performed by J. Nelson and co-workers support this simple model. It is obvious that the effect of electron–electron Coulomb-repulsions and disorder in the site energies can strongly modify the transport characteristics.

We investigated the characteristics of electron transport in electrochemically gated ZnO quantum dot assemblies.[9,12–14] The assemblies were permeated with aqueous and organic

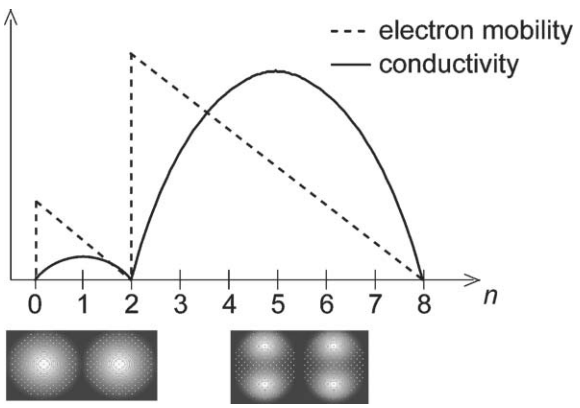

Fig. 9 Expected evolution of the electron mobility (dashed) and conductivity (black) in a solid consisting of semiconductor nanocrystals as a function of the electron number. The plots give only a qualitative picture dealing with the case of weak coupling. The sharp onsets of the mobility are related to transport *via* S orbitals and P orbitals respectively. The decreases in mobility after the onset are due to gradual filling of the S and P orbitals respectively disabling tunneling between a filled and empty orbital of two neighboring quantum dots. The conductivity which is proportional to the product of mobility and electron number shows a peak centered in the S and P bands respectively.

electrolyte solutions. A compilation of results is presented in Fig. 10. The conductance turns on as soon as electrons are injected in the quantum dot film. The conductance rises steeply up to three-four orders of magnitude with increasing accumulation potential within the stability window of the quantum dot solid. With aqueous solvents, the electron number can be as high as ten, due to the effective screening of the electron charge (see above). However, the effect of shell-filling is manifested in a different way than with CdSe quantum dots. The mobility shows a step-like behaviour, instead of the expected peaks (see Fig. 10). The step is located at around $n = 2$. This strongly indicates that the two mobility regimes involve tunneling *via* S and P orbitals, respectively, similar to the case of CdSe assemblies. An insulating state between the S- and P- regimes is, however, not observed. We conjecture that this is due to size dispersion in the ZnO nanocrystals, which is considerably higher (*ca.* 20%) than for CdSe quantum dots (5%). Due to the variation in the energies of the S and P orbitals in the nanocrystal lattice, resonant tunneling between S and P orbitals can also occur to a certain extent, for electron numbers at around two. Furthermore, for electron numbers larger than two, S–P tunneling forms an alternative to the expected P–P tunneling path. This may explain the observation that the S-regime evolves gradually into the P-regime, without a sharp transition. For ZnO nanocrystal assemblies permeated with organic electrolyte solutions, the effects of shell-filling are not so clear, although a sharp onset of the electron mobility is always found (see Fig. 10).

In the case of ZnO nanocrystal assemblies permeated with an aqueous electrolyte solution, the conductance was temperature independent. However, with nanocrystal assemblies permeated with organic electrolyte solutions, the conductance increases with increasing temperature in accordance with Arrhenius-type behaviour, *i.e.* $G \propto \exp(-E_A/k_BT)$; the activation energy, E_A, is of the order of 100 meV, and increases slightly with increasing electron occupation (see Fig. 10). The thermally activated conductance is, very probably, due to the effect of electron–electron repulsion (*i.e.* Coulomb blockade), which is also reflected in the charging characteristics (see Fig. 8). We remark that with CdSe quantum dot solids, a transition between thermally-activated (Arrhenius-type) site-to-site and variable-distance transport (with a different temperature dependence) has been observed.[41]

It is of interest to consider the values of the electron mobility measured in CdSe and ZnO quantum dot solids. Quantitative values of the mobility are obtained from the measured conductance, the electron density in the solid, and the width, length, and height of the gap between the two electrodes. For TOPO-capped CdSe quantum dots cross-linked with heptanediamine, the reported values were low: 10^{-5}–10^{-4} $cm^2\ V^{-1}\ s^{-1}$. The mobility was considerably increased by exchange of TOPO with pyridine and using 1,4-phenylenediamine as a chemical bridge between the nanocrystals (10^{-2} $cm^2\ V^{-1}\ s^{-1}$).[18] The assemblies that we have studied, consisted of uncapped ZnO nanocrystals which assemble into a solid by van der Waals interactions. The values of the mobility measured at room temperature (10^{-2}–10^{-1} $cm^2\ V^{-1}\ s^{-1}$) were

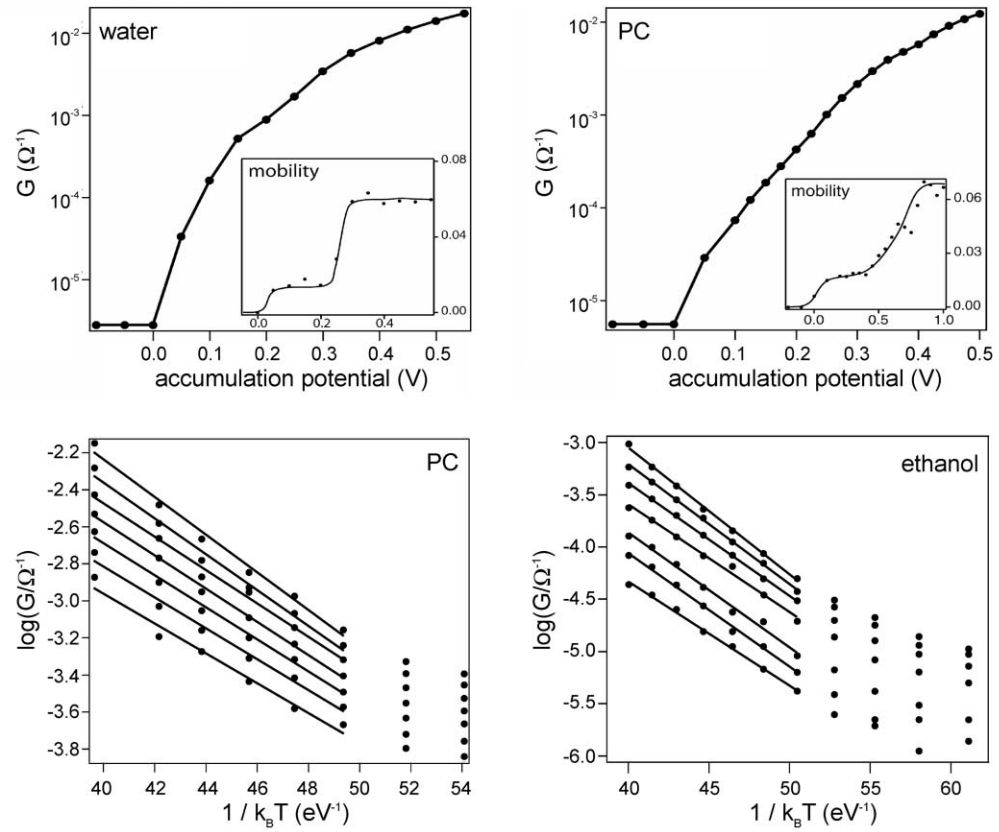

Fig. 10 Characteristics of electron transport in a assembly of ZnO nanocrystals (3.9 nm in diameter) permeated with aqueous and non-aqueous electrolytes. Upper panels: The conductance (measured in the linear response regime) as a function of the accumulation potential. The inserts show the derived electron mobility (in $cm^2\ V^{-1}s^{-1}$) as a function of the accumulation potential. Lower panels: The *T*-dependence of the conductance (conductance plotted *vs.* $1/k_BT$) measured with increasingly more positive accumulation potentials (from bottom to top). The ZnO nanocrystal assembly is permeated with propylene carbonate (PC) (left) and ethanol (right). The activation energies are between 80 ($n = 0.5$) and 100 meV ($n = 3$) for a nanocrystal assembly permeated with PC, and between 100 ($n = 0.5$) and 120 meV ($n = 4$) for an assembly permeated with ethanol.

large compared to those obtained in CdSe assemblies.[9] This must be due to the small width of the tunneling barrier between uncapped ZnO nanocrystals. From the value of the mobility, the tunneling rate and coupling energy between the orbitals of adjacent quantum dots can be obtained using the Einstein–Smoluchowsky equation. In the regime where transport occurs by tunneling between the S-orbitals, we have $\mu_{S-S} = (e/k_BT)\Delta^2\Gamma_{S-S}$, where Δ is the length that has been overcome by the electron in one tunneling step (close to the diameter of the quantum dot). From the experimental mobility $\mu_{S-S} = 0.017\ cm^2\ V^{-1}\ s^{-1}$, we then obtain that the tunneling rate between the S orbitals of adjacent quantum dots $\Gamma_{S-S} = 3 \times 10^9\ s^{-1}$, and the electronic coupling $h\Gamma_{S-S} = 10\ \mu eV$. The coupling energy is a factor thousand smaller than k_BT at room temperature. This shows that the weak coupling regime prevails (see Fig. 6). Weak coupling agrees with the absorption spectrum of the uncharged ZnO nanocrystal assembly which is close to that of non-interacting ZnO nanocrystals.

6. Conclusions and prospects

Quantum-dot solids, consisting of semiconductor nanocrystals can be prepared in a bottom-up approach. High-quality colloidal semiconductor nanocrystals are prepared by wet-chemical methods. These nanocrystals show a remarkable uniformity in their shape and size and surface chemistry and are nearly ideal building blocks for self-assembled quantum dot solids. With electrochemical gating, the electron-occupation of the quantum dot orbitals can be varied in a controllable way, opening the gate to fundamental studies of electronic interactions and transport in these highly versatile artificial systems. An improved control of the structure and the chemical stability remain the important challenges in the chemistry of these systems. Considering the electronic properties, the regime of strong electronic coupling remains to be explored. On the long term, quantum dot solids with controlled and variable electron densities may find applications in the field of opto-electronic switches, LEDs, lasers, and solar cells. However, a lot of challenging problems need to be solved before the engineers will take over. With this brief tutorial review, we hope to have sparked the interest of chemists and physicists in this exciting field of nanoscience.

Acknowledgements

Financial support from EU under "NANOSPECTRA" (research training network, project no. HPRN-CT-2002-00320) is

gratefully acknowledged. Arjan Houtepen and Bernadette Quinn are thanked for insightful discussions.

Daniël Vanmaekelbergh* and Peter Liljeroth
Condensed Matter and Interfaces, Debye Institute, University of Utrecht, Princetonplein 1, 3508 TA, Utrecht, The Netherlands.
E-mail: daniel@phys.uu.nl; Fax: 31 30 253 2403; Tel: 31 30 253 2218

References

1 C. B. Murray, C. R. Kagan and M. G. Bawendi, *Annu. Rev. Mater. Sci.*, 2000, **30**, 545.
2 G. Markovich, C. P. Collier, S. E. Henrichs, F. Remacle, R. D. Levine and J. R. Heath, *Acc. Chem. Res.*, 1999, **32**, 415.
3 C. B. Murray, S. Sun, W. Gaschler, H. Doyle, T. A. Betley and C. R. Kagan, *IBM J. Res. Dev.*, 2001, **45**, 47.
4 A. L. Rogach, D. V. Talapin, E. V. Shevchenko, A. Kornowski, M. Haase and H. Weller, *Adv. Funct. Mater.*, 2002, **12**, 653.
5 M. A. Kastner, *Phys. Today*, 1993, **46**, 24.
6 A. P. Alivisatos, *J. Phys. Chem.*, 1996, **100**, 13226.
7 M. Shim and P. Guyot-Sionnest, *Nature*, 2000, **407**, 981.
8 C. Wang, M. Shim and P. Guyot-Sionnest, *Science*, 2001, **291**, 2390.
9 A. L. Roest, J. J. Kelly, D. Vanmaekelbergh and E. A. Meulenkamp, *Phys. Rev. Lett.*, 2002, **89**, 36801/1.
10 C. A. Leatherdale, C. R. Kagan, N. Y. Morgan, S. A. Empedocles, M. A. Kastner and M. G. Bawendi, *Phys. Rev. B*, 2000, **62**, 2669.
11 A. Germeau, A. L. Roest, D. Vanmaekelbergh, G. Allan, C. Delerue and E. A. Meulenkamp, *Phys. Rev. Lett.*, 2003, **90**, 97401/1.
12 A. L. Roest, A. Germeau, J. J. Kelly, D. Vanmaekelbergh, G. Allan and E. A. Meulenkamp, *ChemPhysChem*, 2003, **4**, 959.
13 A. L. Roest, A. J. Houtepen, J. J. Kelly and D. Vanmaekelbergh, *Faraday Discuss.*, 2004, **125**, 55.
14 A. L. Roest, J. J. Kelly and D. Vanmaekelbergh, *Appl. Phys. Lett.*, 2003, **83**, 5530.
15 P. Guyot-Sionnest and C. Wang, *J. Phys. Chem. B*, 2003, **107**, 7355.
16 C. Wang, M. Shim and P. Guyot-Sionnest, *Appl. Phys. Lett.*, 2002, **80**, 4.
17 B. L. Wehrenberg and P. Guyot-Sionnest, *J. Am. Chem. Soc.*, 2003, **125**, 7806.
18 D. Yu, C. Wang and P. Guyot-Sionnest, *Science*, 2003, **300**, 1277.
19 C. Wang, B. L. Wehrenberg, C. Y. Woo and P. Guyot-Sionnest, *J. Phys. Chem. B*, 2004, **108**, 9027.
20 C. B. Murray, D. J. Norris and M. G. Bawendi, *J. Am. Chem. Soc.*, 1993, **115**, 8706.
21 C. de Mello Donegá, S. G. Hickey, S. F. Wuister, D. Vanmaekelbergh and A. Meijerink, *J. Phys. Chem. B*, 2003, **107**, 489.
22 C. B. Murray, C. R. Kagan and M. G. Bawendi, *Science*, 1995, **270**, 1335.
23 S. F. Wuister, I. Swart, F. van Driel, S. G. Hickey and C. de Mello Donegá, *Nano Lett.*, 2003, **3**, 503.
24 C. J. Kiely, J. Fink, M. Brust, D. Bethell and D. J. Schiffrin, *Nature*, 1998, **396**, 444.
25 E. V. Shevchenko, D. V. Talapin, A. L. Rogach, A. Kornowski, M. Haase and H. Weller, *J. Am. Chem. Soc.*, 2002, **124**, 11480.
26 F. X. Redl, K. S. Cho, C. B. Murray and S. O'Brien, *Nature*, 2003, **423**, 968.
27 R. P. Andres, J. D. Bielefeld, J. I. Henderson, D. B. Janes, V. R. Kolagunta, C. P. Kubiak, W. J. Mahoney and R. G. Osifchin, *Science*, 1996, **273**, 1690.
28 B. O. Dabbousi, C. B. Murray, M. F. Rubner and M. G. Bawendi, *Chem. Mater.*, 1994, **6**, 216.
29 C. Delerue and M. Lannoo, '*Nanostructures: Theory and Modelling*', Springer-Verlag, Berlin, 2004.
30 L.-W. Wang and A. Zunger, *Phys. Rev. B*, 1996, **53**, 9579.
31 I. Kang and F. W. Wise, *J. Opt. Soc. Am. B*, 1997, **14**, 1632.
32 Z. Hens, D. Vanmaekelbergh, E. S. Kooij, H. Wormeester, G. Allan and C. Delerue, *Phys. Rev. Lett.*, 2004, **92**, 26808/1.
33 A. Franceschetti, A. Williamson and A. Zunger, *J. Phys. Chem. B*, 2000, **104**, 3398.
34 M. Shim and P. Guyot-Sionnest, *J. Am. Chem. Soc.*, 2001, **123**, 11651.
35 B. L. Wehrenberg, C. Wang and P. Guyot-Sionnest, *J. Phys. Chem. B*, 2002, **106**, 10634.
36 P. J. M. van Bentum, R. T. M. Smokers and H. van Kempen, *Phys. Rev. Lett.*, 1988, **60**, 2543.
37 U. Banin, Y. Cao, D. Katz and O. Millo, *Nature*, 1999, **400**, 542.
38 E. P. A. M. Bakkers, Z. Hens, A. Zunger, A. Franceschetti, L. P. Kouwenhoven, L. Gurevich and D. Vanmaekelbergh, *Nano Lett.*, 2001, **1**, 551.
39 F. Remacle, *J. Phys. Chem. A*, 2000, **104**, 4739.
40 P. Liljeroth, D. Vanmaekelbergh, V. Ruiz, K. Kontturi, H. Jiang, E. Kauppinen and B. M. Quinn, *J. Am. Chem. Soc.*, 2004, **126**, 7126.
41 D. Yu, C. Wang, B. L. Wehrenberg and P. Guyot-Sionnest, *Phys. Rev. Lett.*, 2004, **92**, 216802/1.
42 K. C. Beverly, J. F. Sampaio and J. R. Heath, *J. Phys. Chem. B*, 2002, **106**, 2131.
43 C. G. van de Walle, *Phys. Rev. Lett.*, 2000, **85**, 1012.
44 S. F. J. Cox, E. A. Davis, S. P. Cottrell, P. J. C. King, J. S. Lord, J. M. Gil, H. V. Alberto, R. C. Vilao, J. Piroto Duarte, N. Ayres de Campos, A. Weidinger, R. L. Lichti and S. J. C. Irvine, *Phys. Rev. Lett.*, 2001, **86**, 2601.
45 R. Parthasarathy, X.-M. Lin and H. M. Jaeger, *Phys. Rev. Lett.*, 2001, **87**, 186807/1.

